© HKL Technology - 2005

2

Microstructural Controls on Trace Element Variability in Ore Minerals

Question: *Does EBSD provide new insight into ore mineral microstructure and the chemical enrichment of elements in hydrothermal ore deposits?*

Introduction

The Witwatersrand gold deposit in South Africa has produced more gold than any other gold deposit in the world, yet its origin has long been the subject of debate. Within the deposit, gold occurs within quartz-rich conglomerate beds in association with the iron sulphide mineral pyrite (FeS_2). The origin of this pyrite is controversial but is fundamentally important in understanding the genesis of the associated gold mineralisation. One particular form of "round" pyrite has been attributed to physical abrasion during sediment transport immediately prior to the deposition of the host sediments. However, chemical alteration (sulphidation) of iron oxides by hot fluids passing through the rock after its original deposition has also been suggested for the origin of the pyrite and associated gold. Discriminating between these models is critical to understanding gold mineralisation processes within this deposit and this requires an appreciation of the complexities of pyrite geochemical heterogeneity. By combining detailed quantitative microstructural analysis of pyrite with intragrain chemical variations, the relationships between rock deformation and chemical alteration within the deposit are being better understood and the nature of gold mineralisation is being revealed.

Detailed optical and atomic number contrast (ANC) imaging of the Witwatersrand pyrite grains indicate localised grain fracturing, often associated with gold mineralisation, within some of the pyrites However, orientation contrast imaging (OCI) and EBSD performed on compact round pyrite grains indicate considerable microstructural complexity within the pyrite. This complexity is related to crystal-plastic deformation of the pyrite.

EBSD Conditions

EXPERIMENTAL SET UP

Study undertaken at Curtin University of Technology, Perth, Western Australia

Sample preparation: polished thin section with a final stage of 0.06μm colloidal silica polishing
SEM type: W filament
EBSD System: HKL CHANNEL 5 with Nordlys II detector
Accelerating voltage: 20 kV

EBSD DETAILS

Grid dimensions: 176 x 184 (Fig. 3); 175x145 (Fig. 5)
Grid spacing: 2 microns
Number of points: 32,384 (Fig. 3); 25,375 (Fig. 5)
Zero Solutions = 6% (Fig 3); 0.2% (Fig. 5)
Mean MAD = 0.6915 (Fig. 3); 0.4435 (Fig. 5)
Noise filtering: Low

© HKL Technology - 2005

Results

Figure 1.

ANC image of large rounded pyrite. Smaller grains of similar greyscale are mostly small pyrite grains. Within the large grain some faints cracks are visible but there is no other discernible microstructure suggesting the grain is compositionally homogeneous with respect to major element geochemistry. An adjacent pyrite grain (upper left) shows a texturally different "spongy" pyrite that contains numerous inclusions.

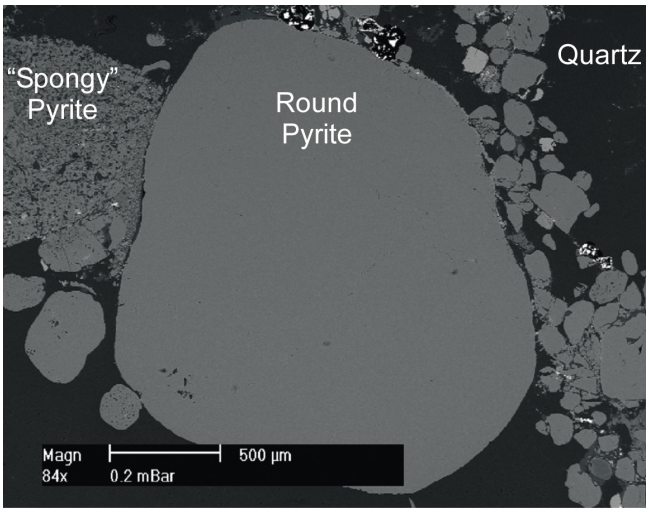

Figure 2.

a) OCI of the large pyrite shown in Fig. 1 indicates significant microstructural complexity associated with intragranular changes in crystallographic orientation of the pyrite (Fig. 2a). White box indicates the position of the map shown in Fig 3a. b) Detail of area of grain shown in Fig. 2a. The microstructure revealed in the OCI is incredibly complex with fine polycrystalline features, sectors and fine bands that were not visible in either the BSE image or by reflected light microscopy. Etching studies by previous workers had noted some internal zonation, that in some cases was truncated, but none of the structures featured here have been previously recorded. White box indicates the position of the map shown in Fig 3a.

a

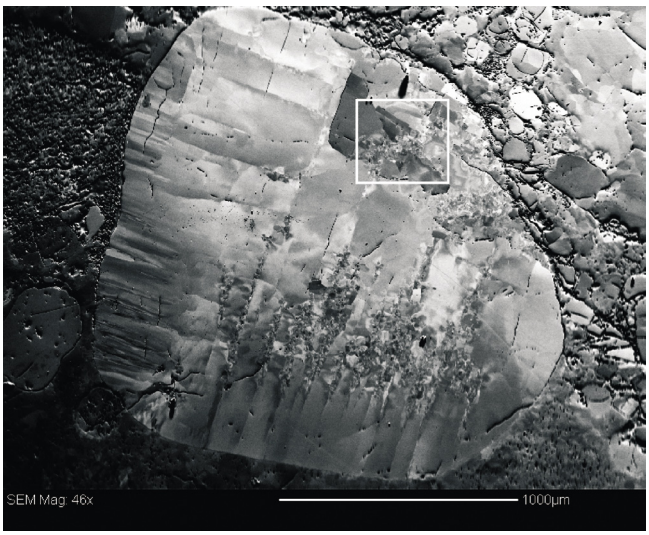

b

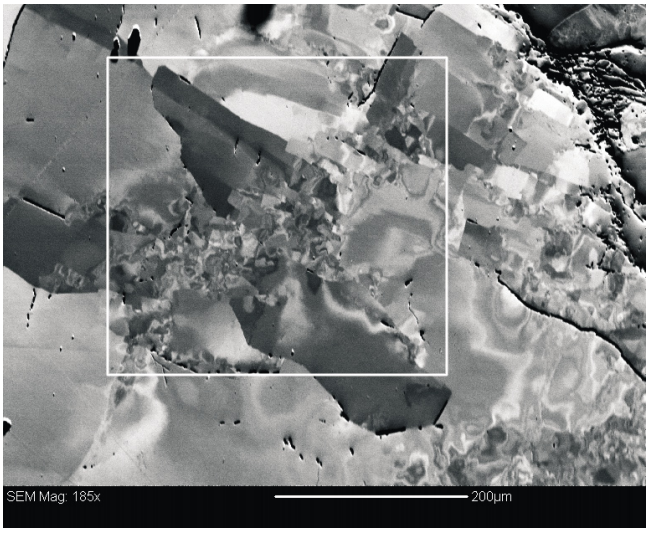

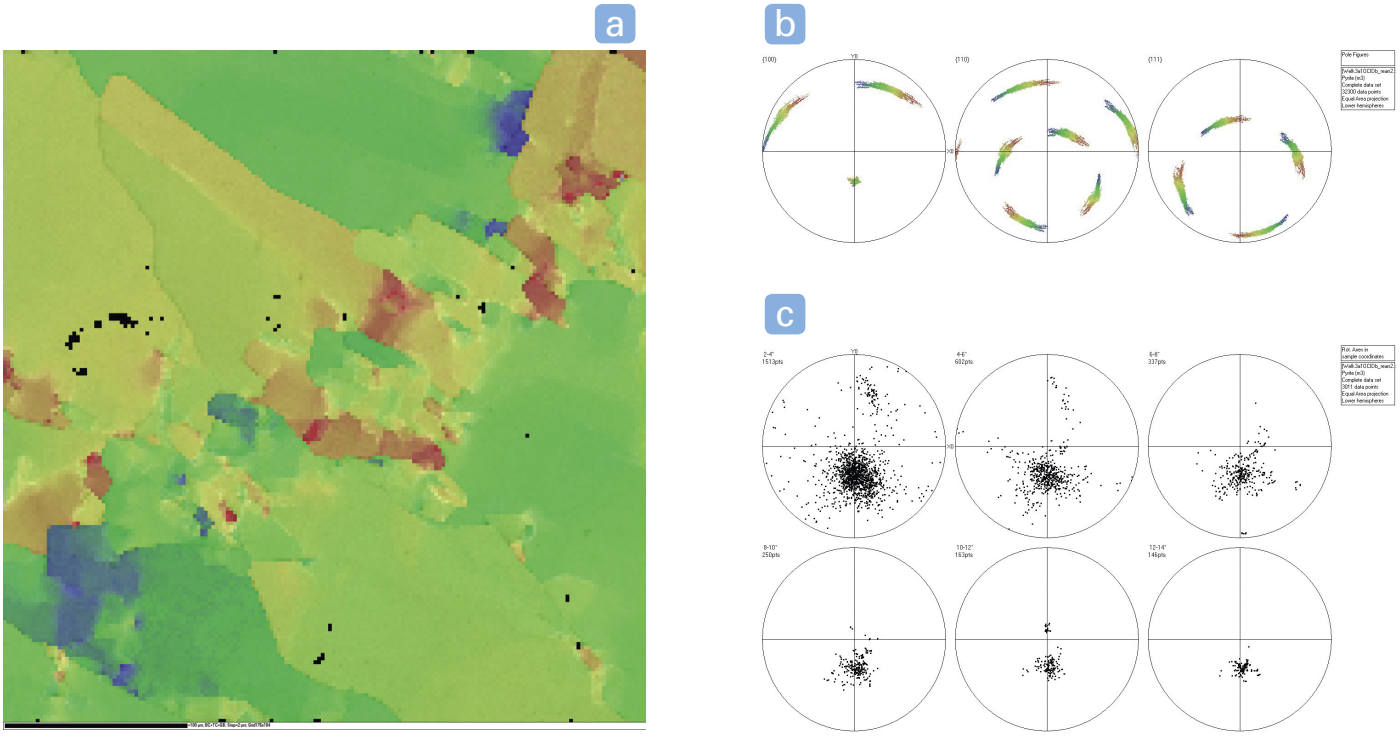

Figure 3.

Quantitative orientation data illustrate some important details of pyrite deformation within the samples. a) EBSD texture component map of the area marked in Fig. 2. Map was created using the automatic mapping facility in Channel 5. Colours represent a relative misorientation of 45° from a pixel in the uppermost blue area of the map. The variations represent recrystallisation of the pyrite in a localised band of deformation. Sides of image represent the sample X (horizontal) and Y (vertical) co-ordinates shown in (b) & (c). b) Variation of crystallographic orientations of pyrite shown in Fig. 3a. Colours correspond to those shown in Fig 3a. Variations are dominated by a small circle distribution associated with a {100} dispersion axis. c) Misorientation axes for (2-14°) associated with the orientation data shown in Figs 3a&b. Despite some variability at small misorientation angles, the main cluster of data from 2-14°correspond to the position of the {100} dispersion axis shown in Fig. 3b. The consistent nature of dispersion and misorientation axes indicates a relationship between crystallographic orientations and active slip systems associated with crystal plastic deformation of the pyrite. Slip systems (for tilt boundaries) can be inferred by assuming the dispersion and misorientation axes are orthogonal to both the slip plane and slip direction of the active slip system. In high symmetry phases such as pyrite the orientation of the trace of the orientation boundary are needed to provide additional constraints on the possible operating slip systems. In this case, the orientation of misorientation boundaries in two directions (approximately the diagonals of Fig. 3a) are consistent with deformation on two {100}<010> slip systems.

© HKL Technology - 2005

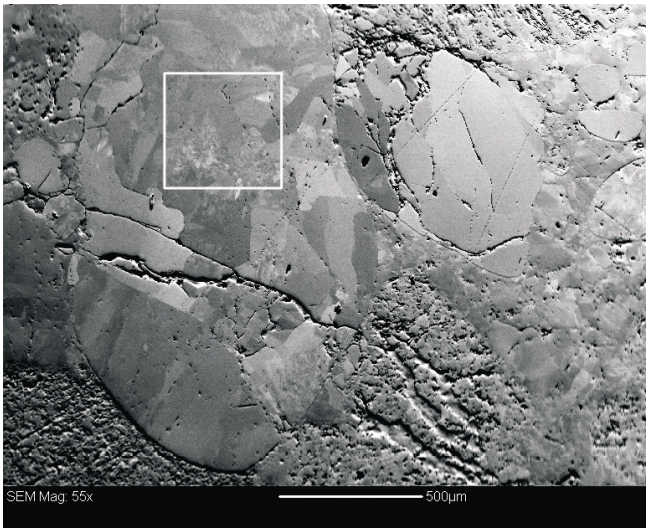

Figure 4.

Similar features to those seen in Figs. 2 & 3 are found in all studied pyrite grains. This second (OCI) example again indicates considerable microstructural complexity within the pyrite. In this case greyscale variations correspond to variations in the crystallographic orientation of domains. The white box corresponds to the area mapped in Fig 5

a

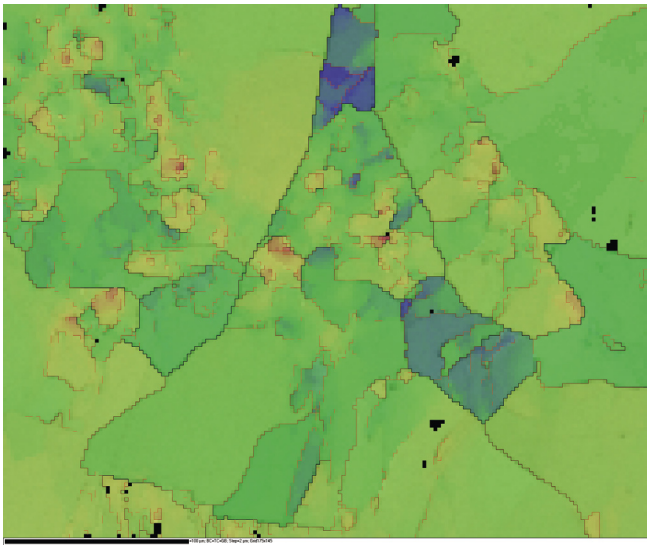

Figure 5.

Automatic EBSD mapping of this grain can be used to quantify the misorientation qualitatively imaged in Fig. 4. a) Variations in crystal orientation (blue to red) shown by a texture component analysis (Max misorientation = 28° from ideal orientation located in the blue area centre-top of image). Interpolated misorientation boundaries (>2° = red; >10° = black) show the development of low angle boundaries within the pyrite. These correspond to changes in the texture component map. Sides of image represent the sample X (horizontal) and Y (vertical) coordinates shown in (b) & (c). b) Pole figures showing the distribution of crystallographic axes in the pyrite of Fig. 5a. Dispersion of data is largely around small circles centred around a {111} pole. However some dispersion is also seen in other directions and are associated with the >10° boundaries shown in b. c) Pole figures indicating 2-14° misorientation axes indicate the main clusters at small angles (<6°) are coincident with the {111} dispersion axis (Fig 5b). However at higher misorientation angles this distribution is less apparent. A similar pattern is seen in the inverse pole figures of misorientation axis data (d).

Figure 5.

b

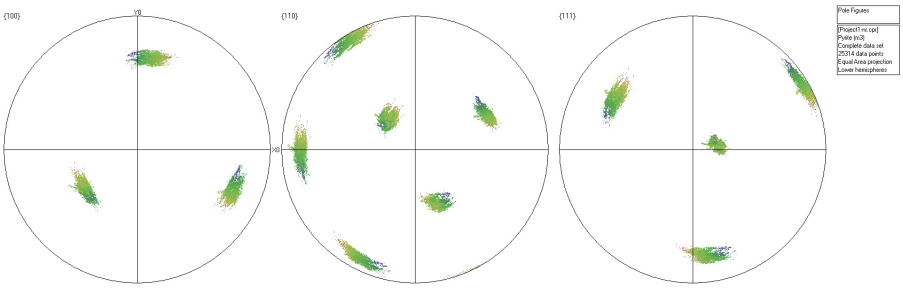
{100}
{110}
{111}
Pole Figures
[Project1-nr.cpr]
Pyrite (m3)
Complete data set
2534 data points
Equal Area projection
Lower hemispheres

c

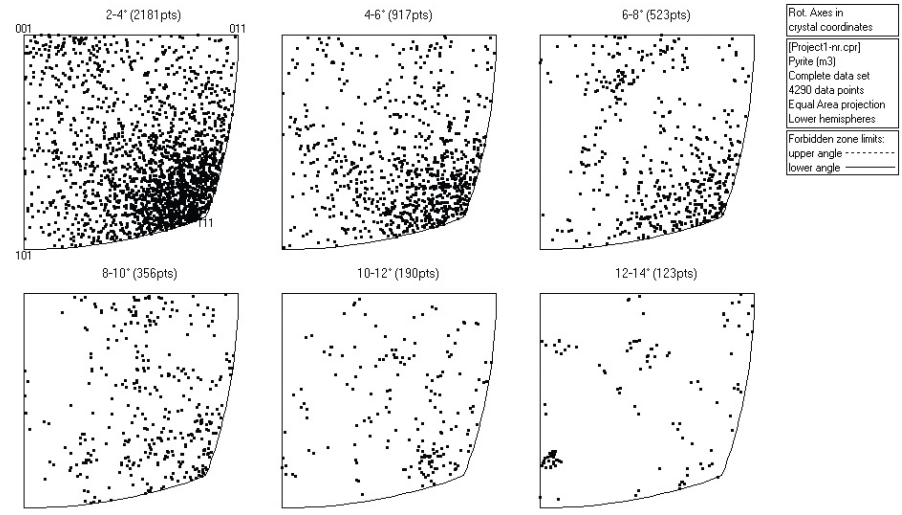
2-4° (2181pts)
4-6° (917pts)
6-8° (523pts)
001
011
111
101
8-10° (356pts)
10-12° (190pts)
12-14° (123pts)
Rot. Axes in
crystal coordinates
[Project1-nr.cpr]
Pyrite (m3)
Complete data set
4290 data points
Equal Area projection
Lower hemispheres
Forbidden zone limits:
upper angle
lower angle

d

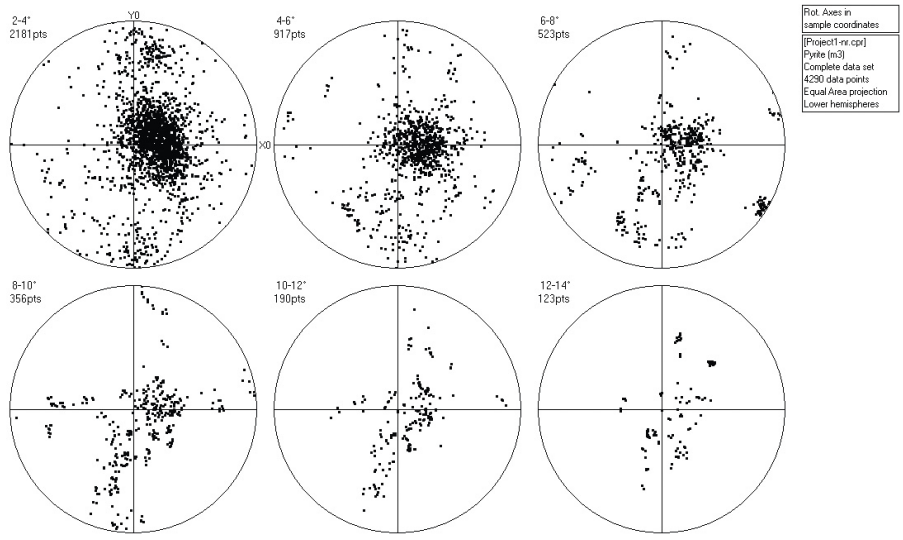
2-4°
2181pts
4-6°
917pts
6-8°
523pts
Y0
X0
8-10°
356pts
10-12°
190pts
12-14°
123pts
Rot. Axes in
sample coordinates
[Project1-nr.cpr]
Pyrite (m3)
Complete data set
4290 data points
Equal Area projection
Lower hemispheres

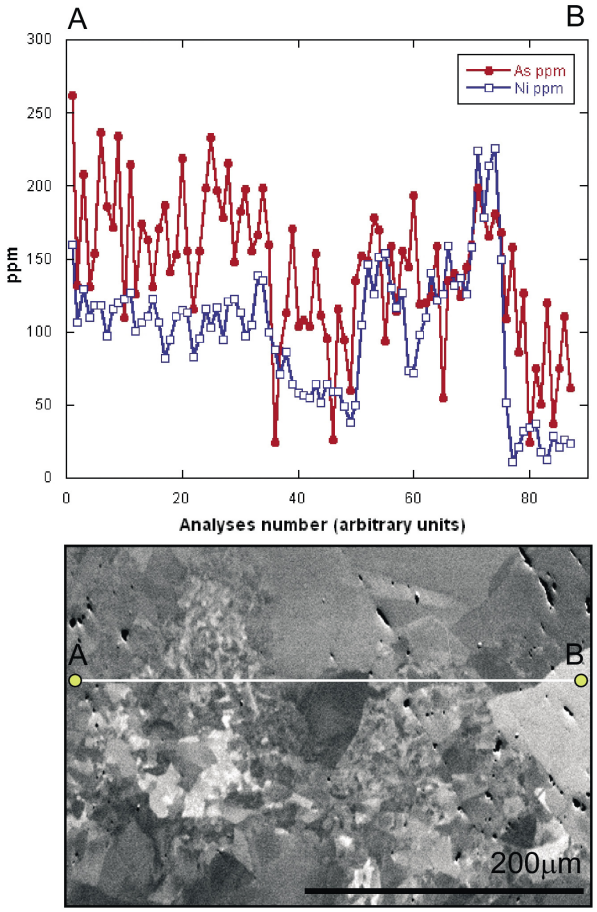

Figure 6.

To assess if these microstructures are significant in modifying pyrite geochemistry electron microprobe analyses across the pyrite shown in Fig 5 has been undertaken. This data indicates that the trace element content for arsenic and nickel changes appreciably across these microstructures with: 1) higher concentrations of Ni and As in zones of high density of small angle misorientations; 2) lower "background" concentrations in relict parts of the original grain (e.g for Ni); and 3) Depletion in As associated with discrete higher angle (c. 10°) misorientation boundaries.

Conclusion

The combined EBSD and OC imaging approach has revealed a complex microstructure to the compact round pyrite grains from the Witwatersrand gold deposit that had not been seen using conventional techniques. These microstructures are associated with crystal-plastic deformation of the pyrite. Preliminary geochemical analyses of the same grains indicate that the microstructure plays an important role in the control of the trace element chemistry.

Answer: *Combined EBSD and geochemical mapping support a model of deformation related chemical modification of the pyrite associated with a late-stage gold mineralising fluid.*

Steven Reddy (Tectonics Special Research Centre, Curtin University of Technology, Perth, Western Australia)
Rob Hough (CSIRO Exploration & Mining, Perth, Western Australia)